Quaternary Science Reviews 30 (2011) 2422–2432

Contents lists available at ScienceDirect

Quaternary Science Reviews

journal homepage: www.elsevier.com/locate/quascirev

Reconstructing the Last Glacial Maximum ice sheet in the Weddell Sea embayment, Antarctica, using numerical modelling constrained by field evidence

A.M. Le Brocq [a,b,*], M.J. Bentley [b], A. Hubbard [c], C.J. Fogwill [a,e], D.E. Sugden [d], P.L. Whitehouse [b]

[a] Geography, College of Life and Environmental Sciences, University of Exeter, Amory Building, Rennes Drive, Exeter EX4 4RJ, UK
[b] Department of Geography, University of Durham, Science Laboratories, South Road, Durham DH1 3LE, UK
[c] Institute of Geography & Earth Sciences, Aberystwyth University, Llandinam Building, Penglais Campus, Aberystwyth, SY23 3DB Wales, UK
[d] School of GeoSciences, University of Edinburgh, Drummond St, Edinburgh EH8 9XP, UK
[e] Climate Change Research Centre (CCRC), School of Biology, Earth and Environmental Sciences, University of New South Wales, Sydney, New South Wales, Australia

ARTICLE INFO

Article history:
Received 8 March 2010
Received in revised form
10 January 2011
Accepted 10 May 2011
Available online 25 June 2011

Keywords:
Last Glacial Maximum
Sea-level
Meltwater pulse
Ice sheet
Ice sheet modelling
Weddell Sea
Antarctica

ABSTRACT

The Weddell Sea Embayment (WSE) sector of the Antarctic ice sheet has been suggested as a potential source for a period of rapid sea-level rise – Meltwater Pulse 1a, a 20 m rise in ~500 years. Previous modelling attempts have predicted an extensive grounding line advance in the WSE, to the continental shelf break, leading to a large equivalent sea-level contribution for the sector. A range of recent field evidence suggests that the ice sheet elevation change in the WSE at the Last Glacial Maximum (LGM) is less than previously thought. This paper describes and discusses an ice flow modelling derived reconstruction of the LGM ice sheet in the WSE, constrained by the recent field evidence. The ice flow model reconstructions suggest that an ice sheet consistent with the field evidence does not support grounding line advance to the continental shelf break. A range of modelled ice sheet surfaces are instead produced, with different grounding line locations derived from a novel grounding line advance scheme. The ice sheet reconstructions which best fit the field constraints lead to a range of equivalent eustatic sea-level estimates between approximately 1.4 and 3 m for this sector. This paper describes the modelling procedure in detail, considers the assumptions and limitations associated with the modelling approach, and how the uncertainty may impact on the eustatic sea-level equivalent results for the WSE.

1. Introduction

Understanding the evolution and behaviour of the Antarctic Ice Sheet (AIS) since the Last Glacial Maximum (LGM) is highly relevant for understanding the future behaviour of the ice sheet in response to future climatic and oceanographic changes. A number of studies have reconstructed the volume and extent of the ice sheet at the LGM, in order to understand the AIS contribution to sea-level change since the LGM (e.g. Denton and Hughes, 1981, see Bentley, 1999 for a summary of pre-1999 efforts, Ritz et al., 2001; Denton and Hughes, 2002; Huybrechts, 2002). In particular, there is interest in the AIS's potential contribution to Meltwater Pulse 1A (MWP1a) at 14.5 ka before present (Fairbanks, 1989; Clark et al., 1996; Hanebuth et al., 2000; Clark et al., 2002; Bassett et al., 2005). LGM ice sheet reconstructions are also important for calculating and removing the Glacial Isostatic Adjustment (GIA) signal in recent geodetic measurements (e.g. from GRACE satellites), in order to estimate present-day ice-sheet mass-balance (Ivins and James, 2005; Ramilllien et al., 2006; Velicogna and Wahr, 2006; Sasgen et al., 2007; Chen et al., 2008; Velicogna, 2009).

The reconstruction of the LGM ice sheet in the Weddell Sea Embayment (WSE) sector of the West AIS (WAIS) has received less research attention than the Ross Sea sector of the WAIS. It has been proposed that the Weddell Sea could have been a large contributor to sea-level change since LGM, and in particular MWP1a (e.g. Bassett et al., 2005, 2007). Previous model reconstructions suggest a significantly expanded and thicker ice sheet in the WSE at the LGM, with the grounding line at the continental shelf break and ice more than 1000 m thicker than present day in the Ellsworth Mountains (Ritz et al., 2001; Denton and Hughes, 2002; Huybrechts, 2002; Pollard and DeConto, 2009). Recent field evidence from the Ellsworth mountains, however, suggests a more modest thickening of the ice sheet in the WSE at the LGM (~230–480 m thicker ice 1000 km from the continental shelf

* Corresponding author. Present address: Geography, College of Life and Environmental Sciences, University of Exeter, Amory Building, Rennes Drive, Exeter EX4 4RJ, UK. Tel.: +44 (0)1392 722257; fax: +44 (0)1392 723342.
E-mail addresses: a.lebrocq@exeter.ac.uk (A.M. Le Brocq), m.j.bentley@durham.ac.uk (M.J. Bentley), abh@aber.ac.uk (A. Hubbard), c.j.fogwill@exeter.ac.uk (C.J. Fogwill), david.sugden@ed.ac.uk (D.E. Sugden), pippa.whitehouse@durham.ac.uk (P.L. Whitehouse).

0277-3791/$ – see front matter © 2011 Elsevier Ltd. All rights reserved.
doi:10.1016/j.quascirev.2011.05.009

break, Bentley et al., 2010, described in more detail below), suggesting either limited grounding line advance or a very low profile ice sheet existing in the embayment.

Resolving this discrepancy between model and field reconstructions is crucial for correctly assessing the contribution of deglaciation of the sector to sea-level rise since the LGM and for providing accurate GIA corrections. The contrast in the extent and thickness of the ice sheet, reconstructed from field evidence and modelling approaches, can be best reconciled by using the available field evidence to constrain the numerical model. It is common practice to calibrate a model with modern observational data, then use this calibrated model to reconstruct past ice sheets. However, it is less common to directly constrain the numerical model using the field evidence, and doing so raises a number of methodological questions, especially when it is a marine ice sheet under consideration.

Bentley et al. (2010) presented the new field evidence from the Ellsworth Mountains and briefly presented reconstructions from numerical ice sheet model simulations for the Weddell Sea Embayment, generated using the hybrid modelling/field evidence driven approach outlined above. The Bentley et al. (2010) paper did not provide significant detail on the modelling approach and the methodological questions raised by the approach, including the assumptions and limitations, which need to be understood when considering the overall conclusion. The aim of this paper is, therefore, two-fold, firstly, to describe the novel approach taken in these simulations in more detail, and secondly to discuss the methodological questions, assumptions and limitations associated with the approach.

This paper will consider the modelling approach taken to integrate the field evidence into the model reconstruction. The marine, terrestrial and ice core evidence available for reconstructing the extent and thickness of the ice sheet at the LGM are summarised, then the model setup and methods used are described. The model results which best fit the field evidence are then presented and the uncertainties attached to the modelling are discussed.

1.1. Approach

There are two major controls on the extent and thickness of a marine-based ice sheet (grounded below sea-level): 1) location of the grounding line and 2) the basal shear stress, which in turn controls the basal sliding velocity of the ice sheet. Surface melting does not have a significant impact in continental Antarctica, so is not a major control. The LGM grounding line location & basal shear stress are both uncertain in the WSE (as discussed below), therefore, one, or both of these, could be adjusted to improve the fit of the numerical model to the field evidence.

The location of the grounding line exerts a strong control over the resulting ice sheet configuration; previous model reconstructions have allowed the grounding line to migrate freely. However, until recently, the physics of the flow transition at the grounding line had not been adequately implemented in a numerical ice sheet model, leading to a large amount of uncertainty in its location. Recent developments have improved the implementation of grounding line migration in numerical models (e.g. Schoof, 2007; Pollard and DeConto, 2009), however, even with these developments incorporated, the location of the grounding line is still dependent on accurate bathymetry data. There are relatively few bathymetric measurements available for the WSE, which hinders the accurate simulation of grounding line migration. For example, Philippon et al. (2006) found modifications to the WSE bathymetry were required to reproduce the present day grounding line following retreat from the LGM. There is also a great deal of uncertainty as to whether the grounding line reached the continental shelf break at the LGM (see section 1.2.1 below). In the WSE, there are two deep troughs which do not extend to the continental shelf break, the deepest of which, the Crary Trough, exceeds 1000 m depth. The lack of erosion may imply that grounded ice did not occupy the outer continental shelf for a long period of time, or was only lightly grounded.

The second method of modifying the extent and profile of an ice sheet is by modifying the basal shear stress. Relatively soft marine sediments exist beneath much of the WAIS, and are thought to be responsible for the fast sliding velocities and low surface slopes that occur in the WAIS (e.g. Alley et al., 1986; Tulaczyk et al., 2000). The low basal shear stress that occurs in these regions allows the ice to maintain high velocities (100 s of m yr^{-1}) despite low gravitational driving stresses. This type of basal sliding is not currently well represented in continental scale ice sheet models, which often have a fixed sliding parameter to represent a range of different bed conditions (see section 2.1 below for an example). The value of the sliding parameter is normally determined by calibrating the present day model prediction to present day ice sheet measurements. However, there is no way to determine the value of this parameter in the currently non-grounded parts of the WSE, and no evidence to support that it may be higher than that which exists beneath the currently grounded ice sheet, in the case of introducing a spatially variable sliding parameter.

Modifying both the sliding parameter, either through varying the single value or introducing a spatially variable parameter, in tandem with the grounding line location would lead to a large number of modelled reconstructions, potentially with a high degree of equifinality. It is likely that a similar result will be achieved through both approaches suggested above. Assuming this is the case, given the level of uncertainty over grounding line physics, its former location and the input bathymetry data, the simulations described in this paper examine only the LGM grounding line position required for the ice sheet model to reproduce the appropriate amount of thickening to match the LGM field evidence. The sliding parameter in the areas not currently covered by grounded ice is not adjusted beyond the values that reproduce the present day calibrated ice sheet prediction. The implications of this approach is discussed further in Section 6.

1.2. Field evidence

1.2.1. Marine geological data

The southern Weddell Sea is notoriously difficult to work in, with extensive first- and multi-year sea-ice blocking access for most research vessels. For this reason there have been only a few marine geological studies of the region. There are undoubted glacial-marine sediments and tills close to the shelf break and even in the deep ($\sim$1000 m) Crary Trough (Fig. 1), implying extensive grounding line advance *at some point*, but attempts to date the limited number of cores from here have been problematic. For example, Elverhoi (1981) provided short cores from the shelf break and upper continental slope in the southern Weddell Sea. These were of glacial-marine mud, dated to 31 to >35 ka, but were subject to iceberg disturbance (Bentley and Anderson, 1998) and strong current scouring (Anderson et al., 1979). Anderson et al. (1980) attempted to date cores from the shelf west of Crary Trough but this suffered from age inversions, also due to iceberg reworking. Thus, the age of the last glacial occupation of the Crary Trough and continental shelf immediately west of the trough remains enigmatic. Further east, there is evidence for advance of the East Antarctic Ice Sheet (EAIS) margin during the last glacial cycle but retreat was underway by 26 ka, earlier than the LGM (Anderson and Andrews, 1999).

Bentley and Anderson (1998) provided the first synthesis of marine and terrestrial data in the WSE in order to develop a field-based reconstruction of the LGM ice sheet in the region. On the

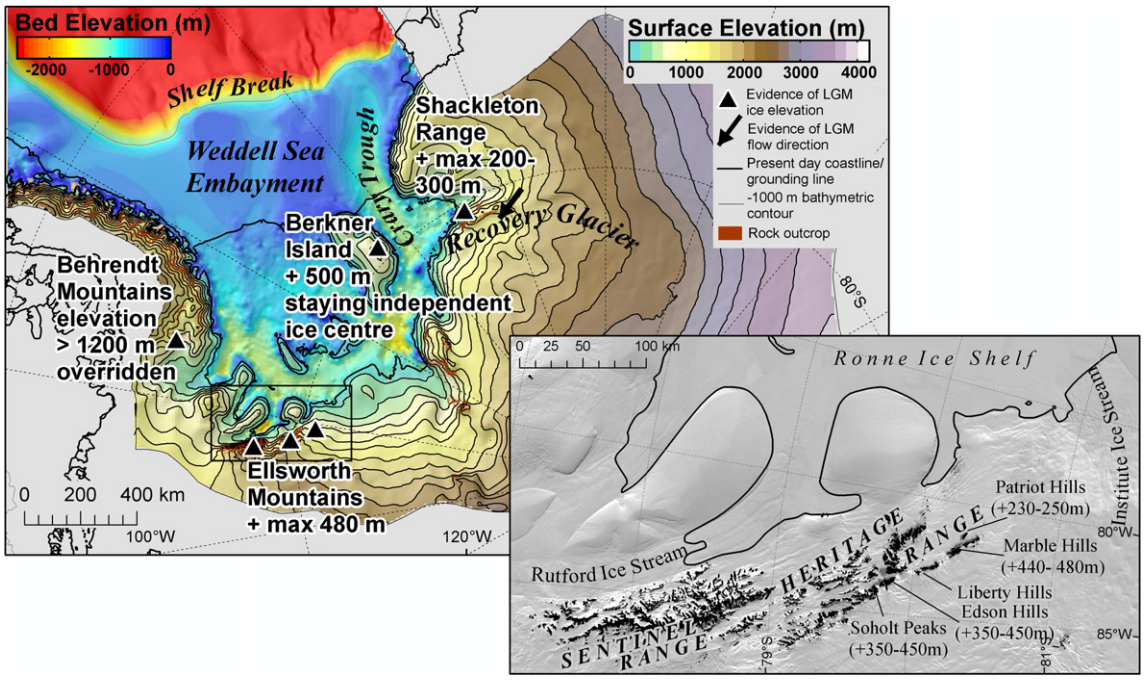

Fig. 1. Location map and summary of LGM field evidence, inset shows new field evidence (elevation of trimline above present day ice sheet) and locations for the Ellsworth Mountains.

basis of the limited data available their reconstruction inferred an advance to the shelf break – as found along much of the Antarctic margin elsewhere – but they noted that the age of glacial deposits at the shelf break was unknown.

1.2.2. Terrestrial glacial geology data

The Bentley and Anderson (1998) reconstruction used terrestrial glacial geological data from the southern and western rim of the WSE. This included the evidence of a prominent erosional trimline in the Ellsworth Mountains, which reaches elevations of 3000 m on the inland faces of the Sentinel Range (Fig. 1, inset), and ~1800 m on the ice shelf facing sides of the southern Heritage Range (e.g. Liberty Hills) (Denton et al., 1992). The trimline is discontinuous in the Heritage Range, occurring only on the upper parts of the highest peaks. It is not observed in the Marble Hills (southern Heritage Range), for example, leading Denton et al. (1992) to the conclusion that the thicker ice sheet covered all but a few high peaks of the northern Heritage Range. Present day ice elevations on the inland side of the Sentinel Range are around 2000–2200 m, descending to only 1000 m on the ice shelf facing sides of the Liberty Hills (only ~150 km from the present day grounding line of the Institute Ice Stream). The Denton et al. (1992) trimline is approximately ~800 m above the present day ice sheet. This trimline – marking the former surface of the ice sheet – is undated but Denton et al. (1992) proposed two alternative age models. They argued that it could either be LGM in age or that it may in fact be much older, possibly pre-Quaternary. Reconstructions since then have widely adopted the LGM age 'model' (Bentley and Anderson, 1998; Bentley, 1999; Ivins and James, 2005), and this has provided an important constraint on ice sheet reconstructions in the region.

More recently, Bentley et al. (2010) mapped a second limit, this one a depositional trimline, which is significantly lower than the mapped Denton et al. (1992) trimline. The trimline in the Heritage Range is a maximum of 440–480 m above present-day ice sheet in the Heritage Range (ice shelf facing sides, see Fig. 1, inset for trimline elevations throughout the Heritage Range). The trimline is most prominent in the Marble Hills, but is observed as a less continuous feature in the Patriot Hills, ~230 m above present day ice. With the advent of cosmogenic isotope analysis for surface exposure dating, it is possible to date the glacial geological features in the Ellsworth Mountains. ^{10}Be analyses on erratic boulders show that the lower trimline likely dates to the LGM and that the WAIS has thinned progressively since about 15 ka to present. The implication is that the LGM WAIS ice surface in the Ellsworth Mountains was substantially lower than previously assumed (Bentley et al., 2010).

In the Shackleton Range the Bentley and Anderson (1998) reconstruction used geomorphological evidence of ice over-riding at the western end of the range to infer ~1000 m of LGM thickening of the WAIS. However, Fogwill et al. (2004) demonstrated that the summits of the range have been ice-free for >1 Ma and suggest that a more probable LGM position is provided by, as yet undated, lateral moraines that lie 200–340 m above present-day ice at the western end of the range (see also Höfle and Buggisch, 1995)

In the southern Antarctic Peninsula, Bentley et al. (2006) demonstrated that ice overtopped summits > 500 m above present ice (e.g. Behrendt Mountains), so were only able to provide minimum estimates for LGM thickness.

1.2.3. Glaciological data

The recently-drilled 948 m long Berkner Island ice core encompasses the last glacial cycle and has important implications for WSE glacial history (Mulvaney et al., 2007). Firstly, isotopic values in the lower parts of the core are all entirely consistent with locally-derived accumulation, and show that ice from the continental interior has not been advected over the site. The implication is that Berkner Island was not over-ridden by either the West or East Antarctic Ice Sheets during the last glacial cycle. Rather, it remained an independent ice rise and centre of ice accumulation throughout the last glacial cycle (Mulvaney et al., 2007). Analysis of the ice core suggests that during the LGM ice at the Berkner Island site was ~500–900 m thicker than at present (R. Mulvaney, pers.comm. Jan, 2011).

Analysis of internal radar layers in Coats Land (eastern sector of the WSE) by Rippin et al. (2006) suggests modified flow in the

tributaries of the Recovery and Slessor glaciers at the LGM. The evidence does not support a greatly expanded ice sheet however, with the overall flow direction requiring an ice sheet morphology and flow direction similar to that of today (roughly E–W), rather than that predicted by the model of Huybrechts (2002) (roughly S–N).

Thus, the glaciological evidence and terrestrial glacial geology all point to a thinner LGM ice sheet in the WSE than previously assumed. The evidence outlined here is summarised in Fig. 1, and will be used to constrain the numerical model, in order to produce a modelled reconstruction which is consistent with the field evidence.

2. Model description

2.1. Ice dynamics

This paper employs the Glimmer ice sheet model (Rutt et al., 2009), which is based on the model of Payne (1999). For more comprehensive information on the model, the reader is referred to Rutt et al. (2009) or Payne (1999); only the key differences from the model setup in Payne (1999) are described here.

One key difference from the model applied by Payne (1999) is the method of calculating the sliding velocity. Previous attempts to model the AIS have used either a 'hard-bed' sliding relation (following Weertman, 1964), or a 'soft-bed' sliding relation (e.g. Budd et al., 1984; Huybrechts, 2002). The hard-bed sliding relation considers the sliding velocity (u_B) to be a linear function of the basal shear stress (considered equivalent to the gravitational driving stress),

$$\begin{aligned} \boldsymbol{u}_B &= -B_t \rho_i g H \nabla s \quad \text{if } T_B = T_{pmp} \\ \boldsymbol{u}_B &= 0 \quad \text{if } T_B < T_{pmp}, \end{aligned} \tag{1}$$

where B_t is the traction parameter, ρ_i is ice density (917 kg m^{-3}), g is acceleration due to gravity, H is ice thickness, s is the ice surface elevation, T_B is the basal ice temperature and T_{pmp} is the pressure melting temperature. This hard-bed type of sliding relation produces a convex ice surface profile with steep slopes at the margins of the ice sheet (e.g. Vialov, 1958). Using Eq. (1) as the sole sliding relation for the present-day AIS can lead to modelled ice thicknesses in excess of 1000 m thicker than the existing ice sheet in WAIS low profile areas, where the surface is drawn down by fast flowing ice streams.

To avoid this problem, a soft-bed sliding relation can be used, incorporating the inverse of ice thickness above buoyancy (H^*) as a proxy for the effective pressure

$$\begin{aligned} \boldsymbol{u}_B &= \frac{-B_s \rho_i g H \nabla s}{H^*} \quad \text{if } T_B = T_{pmp} \\ \boldsymbol{u}_B &= 0 \quad \text{if } T_B < T_{pmp}, \end{aligned} \tag{2}$$

where B_s is a sliding parameter and H^* is given by

$$H^* = H + (\rho_w/\rho_i)h, \tag{3}$$

where ρ_w is the density of sea water (1028 kg m^{-3}) and h is the bedrock elevation. Incorporating H^* into the sliding relation allows the typical concave surface profiles of the WAIS to be reproduced. Despite only being a proxy representation of soft-bed sliding, Eq. (2) can reproduce the low profile slopes present near the grounding line of the WAIS. However, when a value of B_s appropriate for reproducing WAIS ice streams is used, the inland parts of the EAIS are predicted to be up to 500 m too low in elevation. It is logical therefore to apply Eq. (1) where hard bed sliding occurs, and Eq. (2) where soft bed sliding occurs. Unfortunately the distribution of water saturated deformable sediments is not fully known for the whole AIS. In this paper, as a fairly crude first approximation, where the bed is above sea-level (unrebounded) the ice is considered to flow via hard bed sliding. Where the bed is below sea-level, where deformable marine sediments are most likely to occur, it is considered to flow via soft-bed sliding.

As indicated in Eqs. (1) and (2), sliding only occurs where the base of the ice is at the pressure melting point. This criterion is implemented in order to restrict fast ice flow to the ice streams, where frictional heating maintains the basal ice at the pressure melting point (Payne, 1999). Slow flowing inter-stream regions occur because the region cannot maintain a melt rate high enough to keep the ice at the pressure melting point. Again, this is a fairly crude approximation because it does not include the role of subglacial water flow in maintaining the ice at pressure melting point in areas of net basal freeze-on rate; also, slow ice flow is also known to exist where the ice is at pressure melting point (Siple Coast region, Joughin et al., 2004). However, the criterion does allow the present day ice sheet surface to be reproduced successfully.

One further difference from the model setup of Payne (1999) is the value of the geothermal heat flux (G), here taken to be -70 mW m^{-2} (following Joughin et al., 2004; Maule et al., 2005) compared to -42 mW m^{-2} in Payne (1999). Table 1 shows the values of the parameters that are different to, or not specified in Payne (1999).

The best-fit values for B_t and B_s were found by calibrating the predicted ice sheet surface with a measured ice sheet surface, with particular emphasis on reproducing the low slopes and high velocities of the fast flowing ice streams draining the ice sheet. The calibrated parameter values will in part reflect the buttressing effect of the ice shelves (though they are not explicitly represented here), and a minimum value of H^* (50 m) is imposed in equation (2), restricting the maximum velocity at the margins.

2.2. Isostasy

For the present day experiments (Section 4), the unrelaxed basal topography (see below) is used for all experiments. Isostatic adjustment is included in the LGM experiments (Section 5), using a simple elastic lithosphere model (with a flexural rigidity, D, see Table 1), and a relaxing asthenosphere model (with a relaxation time, τ), following Lambeck and Nakiboglu (1980) and Hagdorn (2003).

3. Model setup

3.1. Configuration

The WSE domain was defined using flow routing algorithms and consideration of the ice surface slope to determine the location of ice divides (derived from an ice surface Digital Elevation Model (DEM), Bamber et al., 2009; Griggs and Bamber, 2009). Limiting the domain to the WSE allows a higher resolution domain to be used than would be possible if modelling the entire AIS. Limiting the domain also means that the location of the grounding line in other sectors of the WAIS can be ignored, although this makes the assumption that the WAIS ice divide at the LGM was at the same location as the present day ice divide. The domain resolution used

Table 1
Table of values (extra from/different to Payne, 1999).

Parameter	Value	Units	Reference
G	-70	mW m^{-2}	Joughin et al. (2004)
B_t	10^{-5}	m yr^{-1} Pa^{-1}	–
B_s	1	m^2 yr^{-1} Pa^{-1}	–
D	10^{25}	Nm	Le Meur and Huybrechts (1996)
τ	3000	Years	Le Meur and Huybrechts (1996)

in this paper is 10 km, allowing individual flow features, and the mountainous areas to be better resolved.

The basal topography is provided by the BEDMAP dataset (Lythe et al., 2001). The original dataset is available at a 5 km resolution; when this is resampled to the 10 km model domain, the mountain peaks are reduced in elevation through the smoothing inherent in the resampling technique. The reduced elevation of mountainous areas will affect ice flow in the locality of the Ellsworth Mountains in particular, which represent a large barrier to ice flow. Rather than assign the maximum sub-grid value (e.g. Payne and Sugden, 1990) to the DEM, which may over-predict the mountain height in the 10 km cell, one standard deviation was added to the DEM in ice free areas. This takes into account the morphology of the sub-grid topography; if the grid cell is largely one height with a peak, little elevation will be added, whereas if the sub-grid morphology is complex, with a greater percentage of higher elevations, a larger elevation will be added. The standard deviation of the sub-grid elevations were calculated from the 1 km Radarsat Antarctic Mapping Project (RAMP) surface DEM (Liu et al., 1999, surface topography is equivalent to the bed topography in ice free regions). The rock polygon dataset from the ADD (Antarctic Digital Database) v5 was used to define 'ice free' cells, i.e. cells which contain greater than 15% rock according to the ADD rock polygon data.

The BEDMAP dataset was also further modified by incorporating the inferred bed topography of Le Brocq et al. (2008) in the region of Recovery Glacier (EAIS). Le Brocq et al. (2008) suggest complex topography and a large area of the bed below sea-level in this region, inferred from surface terrain analysis. The present-day ice sheet model predictions with and without this modification are presented in Section 4.

The ice flow model was initialised using the present day ice sheet surface DEM and the temperature model was initialised using a quadratic temperature-depth profile using the pressure melting point and the surface temperature as the boundary conditions.

3.2. Model domain setup

A gridded mask for the present day ice sheet extent was created using the ADD v5 coastline dataset in order to delimit the grounded ice regions. The ice thickness in the grounded/floating ice boundary cells was set to flotation in order to constrain the ice elevation at, and location of, the grounding line.

A series of grounded-ice-extent masks were created for the LGM experiments, in order to investigate the modelled (equilibrium) LGM grounding line location that leads to the ice sheet elevation to match the available field evidence. The method for creating these is described in Section 3.4.

A further mask was created in order to delimit the inland ice sheet catchment boundaries. A zero-flux artificial boundary was created, whilst this artificial boundary may have an impact on the predicted surface, the bias introduced will be consistent across the present day and LGM predictions, and should not impact on the final sea-level contribution calculations.

3.3. Climatic forcing

The model requires two climatic inputs; the mass balance and the surface temperature. For the AIS the mass balance is considered to be equivalent to accumulation, and the surface temperature is a required boundary condition for ice sheet temperature evolution.

The present day accumulation dataset used in this paper is that of Arthern et al. (2006), resampled from its original resolution of 25 km to the model domain resolution of 10 km. Little is known about the accumulation pattern at the LGM, however limited ice core records suggest that LGM accumulation was approximately half that of the present day value (e.g. Parrenin et al., 2007; Ruth et al., 2007). Therefore, the LGM accumulation forcing used is half the present day distribution. The original Arthern et al. (2006) dataset is confined to the present day ice sheet/shelf extent. If the LGM ice sheet was more extensive than the present ice shelf, data are needed for a wider region. In the WSE there is a distinct east-west gradient in the accumulation values, therefore, it is important that this is maintained in an interpolation algorithm. A global interpolation algorithm (power 10), implemented in ArcGIS, was found to reproduce the pattern most successfully and this was merged with the original data to produce an accumulation dataset covering the continental shelf.

Surface temperature measurements are available for the period 1982–2004 (described in Comiso, 2000). The mean annual surface temperature for this period was plotted against the surface elevation and a quadratic trendline fitted to the data in order to derive a temperature lapse rate:

$$T_s = 1.513 \times 10^{-6} s^2 - 4.014 \times 10^{-3} s - 18.55, \quad (4)$$

where T_s is the surface temperature.

The temperature difference between present day conditions and the LGM has been derived from a number of ice core isotope records. The temperature difference is consistently found to be around 8–9 °C lower at the LGM than present day (Jouzel et al., 1987 (Vostok), Steig et al., 2000 (Taylor Dome), Stenni et al., 2001 (Dome C), Taylor et al., 2004 (Siple Dome)). The surface temperature is calculated at each model timestep, using Eq. (4) and the ice sheet elevation, and is lowered by 9 °C for the LGM experiments.

3.4. Grounding line advance algorithm

As the grounding line location is fixed in the model setup, a suite of possible LGM grounding line locations need to be constructed. Experiment 1 locates the grounding line at the continental shelf break, in order to repeat previous (over-estimated) reconstructions. A further set of experiments (2–10) consider less extensive LGM grounding lines, driven by an enclosure-based grounding-line advance algorithm, explained in this section.

The algorithm recreates grounding line advance independent of the ice sheet model, in order to produce a series of masks with varying levels of grounding line advance with which to delineate the grounded ice domain. The algorithm begins at the present day ice extent and advances the grounding line over time, until the entire continental shelf is designated grounded ice. Snapshots at specified points in time were extracted to provide a series of grounding line masks (Fig. 2). In each case, the modelled ice sheet, once run to equilibrium using this mask, was compared to the field data (Fig. 1).

First, the areas where grounded-line variation is likely to occur were identified. There are two major troughs which occur on the continental shelf in the WSE (Fig. 1). It is in these troughs that fast flow features are likely to occur, whether these are ice streams/plains or shelves and, hence, the majority of the grounding line variation will occur. The presence of fast flow features will also result in restricting grounding line advance from the western and eastern edges (slower flowing regions) of the WSE. However, there is nothing to stop the ice sheet grounding into the central part of the continental shelf.

The grounding line was therefore allowed to advance only from areas of the grounded ice sheet where the basal topography is deeper than 500 m below sea-level (b.s.l.) (generally high flux ice stream regions), into areas of bathymetry which are also deeper than 500 m b.s.l. (delimiting the troughs successfully). Grounding line advance in other regions is assumed to be restricted by the presence of fast flowing, floating or barely grounded ice. Therefore,

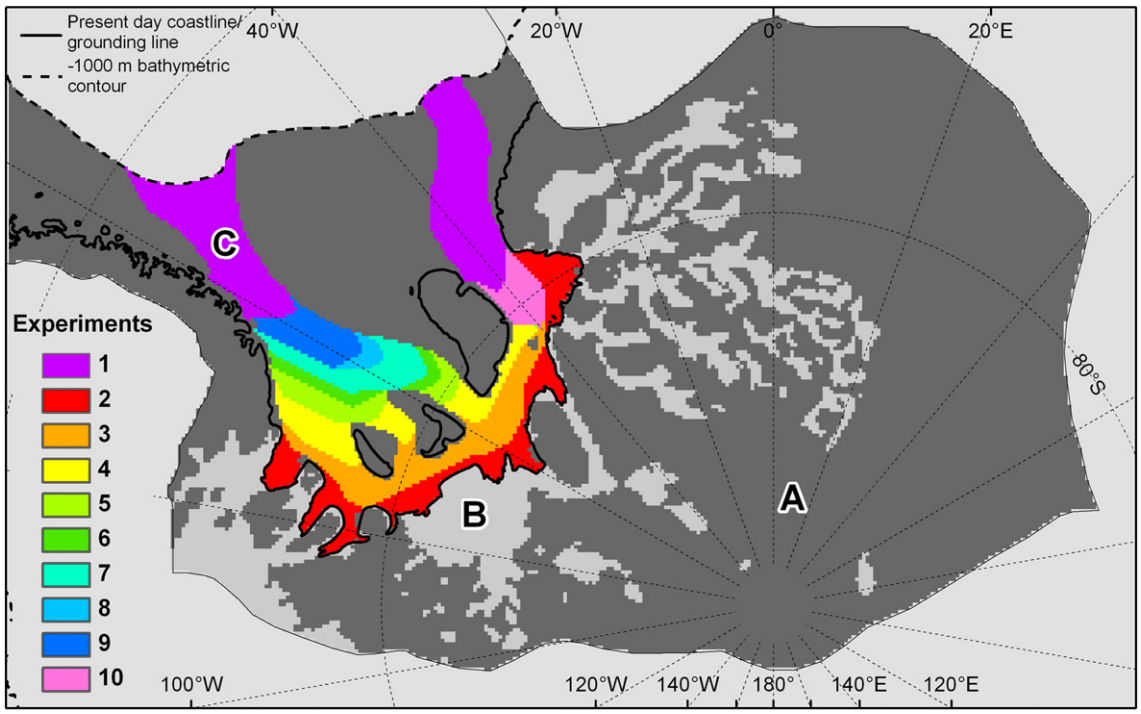

Fig. 2. Grounding line advance algorithm mask (A–C categories described in text, C includes all coloured regions) and the suite of grounding lines implemented (1–10). Excluding Experiment 1, each experiment includes the area grounded in the previous experiment; for example, Experiment 3 includes the area already grounded in Experiment 2.

the WSE domain was divided into three categories; A) grounded ice with its bed shallower than 500 m b.s.l., with no advance allowed, B) grounded ice with bed deeper than 500 m b.s.l., with advance allowed and C) ungrounded/ice free areas with bed deeper than 500 m b.s.l., where the grounding line variation is allowed. The resulting mask was 'smoothed' around the edges of the grounded ice, in order to produce a coherent grounding line (Fig. 2).

Once the category mask is created, the algorithm analyses the degree of enclosure of each cell falling into category C above. The basis of using an enclosure criteria relates to the existence of 'pinning points' which provide back stress for ice shelves, slowing their flow and causing them to become grounded. The more enclosed a cell is, the more likely it is to become grounded. The degree of enclosure of each cell is considered at every timestep: if the cell has four or more ice covered neighbours (A or B above), the cell becomes ice covered. The grounding line is then advanced in this manner over a number of timesteps until the grounding line reaches the continental shelf break, with snapshots taken at given time intervals to create the series of masks. The extent of the grounding line advance in the different troughs can be controlled separately.

Similar grounding lines have previously been produced in the WSE from an independent approach; from the model of Pollard and DeConto (2009). The model incorporates dynamic grounding line migration, and is used to reconstruct the AIS over the past five million years. A snapshot from 1.094 Myr ago looks similar to some of the grounding lines tested in this paper, suggesting the algorithm presented here can produce results similar to a model with a full transient, freely evolving grounding line.

3.5. Conversion of ice volume change into eustatic sea-level change

The ice volume change between the LGM and present day ice sheets is here converted into equivalent *eustatic* sea-level change. Here we follow the definition of Farrell and Clark (1976) where eustatic sea-level change (E) is simply:

$$E = \Delta V / A, \tag{5}$$

where ΔV is the change in the ocean volume, and A the global ocean area. Gravitational effects and solid Earth deformation are not accounted for in the calculation, i.e. we just consider the change in ocean water volume, and not the change in the capacity of the ocean basins. Observed relative sea level change in a given geographical location will differ from the quoted eustatic value due to local isostatic/GIA effects.

Converting the reconstructed LGM ice volume into an equivalent eustatic sea-level change is less straightforward for a marine-based ice sheet than for a land-based ice sheet, and needs to take into account the fact that some of the ice has already displaced ocean water. The total change in volume of ocean water (ΔV) is, therefore, the difference between the water-equivalent volume of ice *not displacing ocean water* at the LGM and present day. The 'volume of ice not displacing ocean water' corresponds to the ice thickness above buoyancy. The ice thickness above buoyancy was calculated for the present day and LGM ice sheets using Eq. (3), using LGM sea-level (−120 m) and depressed bed elevation for the LGM calculation. The difference was then converted into water-equivalent using an ice density of 917 kg m^{-3} and a (fresh) water density of 1000 kg m^{-3}, then converted to eustatic sea-level using Eq. (5) and an assumed global ocean surface area of 3.64×10^{14} m^2 (Philippon et al., 2006).

4. Present day results

The present day measured ice sheet surface and velocity in the WSE (Fig. 3a and b) exhibits a number of features that need to be represented by the ice sheet model in order to have confidence in the LGM predictions. The model must firstly be able to reproduce the low elevations, low surface slopes and high velocities of the major ice streams feeding the ice shelf. The model must also represent the slow flow regions of the EAIS well, as a thinner/

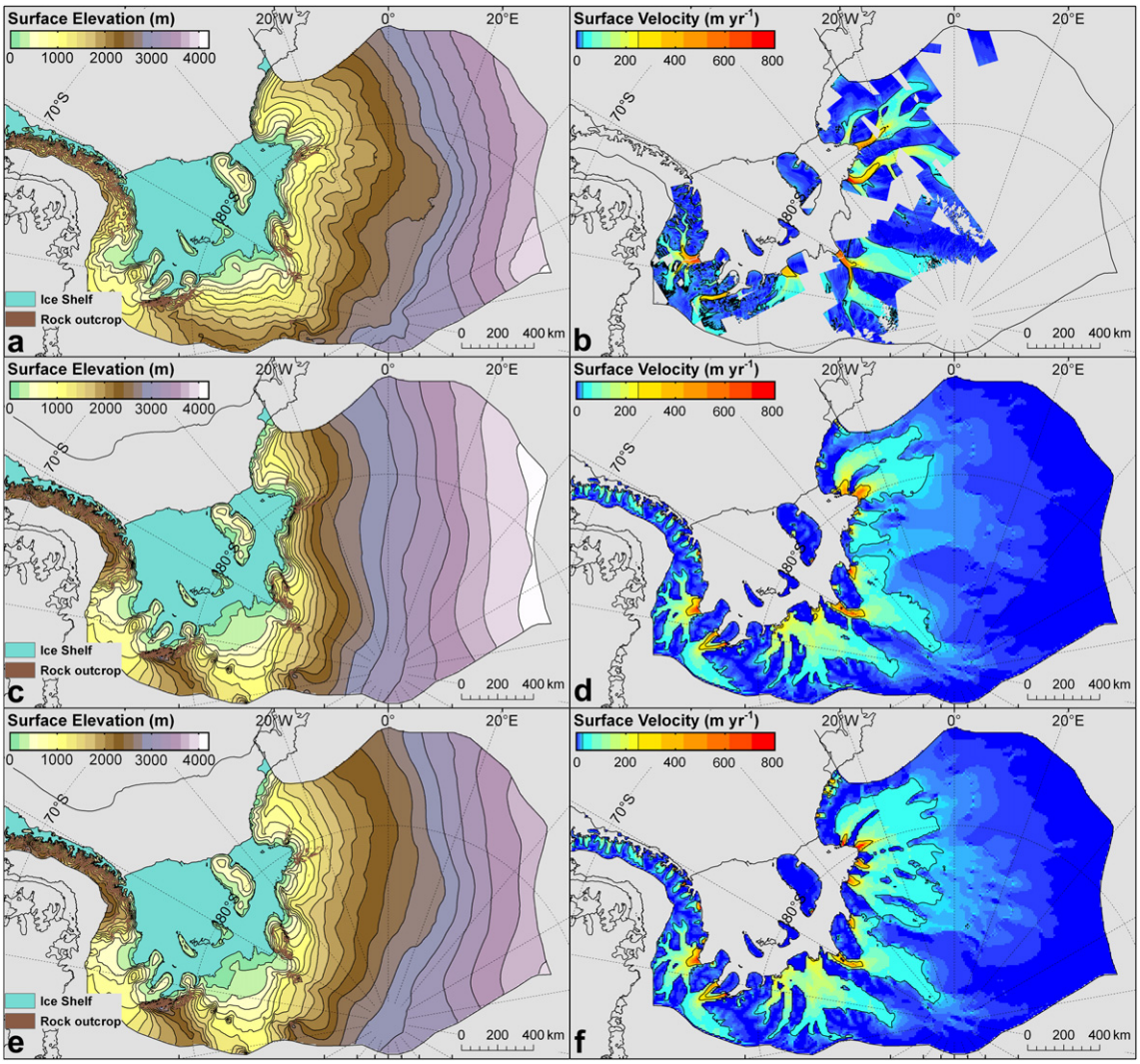

Fig. 3. Present day results; a) measured surface elevation, b) measured surface velocity, c) modelled surface elevation (original BEDMAP dataset), d) modelled surface velocity (original BEDMAP dataset), e) modelled surface elevation (modified BEDMAP dataset), f) modelled surface velocity (modified BEDMAP dataset).

thicker inland ice sheet will also impact on the sea-level equivalent contribution of the WSE. Finally, the elevation around the mountainous regions where field evidence exists, particularly the Ellsworth Mountains and the Shackleton Range, must be accurate in order to reliably constrain the LGM comparison with the present day ice sheet configuration.

The ice sheet resulting from the original BEDMAP dataset (Fig. 3c and d) shows good agreement with the measured ice sheet in the WAIS half of the domain, exhibiting low slopes and high velocities in the ice streams in locations which match measured ice streams well. The ice rise elevations are also in good agreement (e.g. Berkner ice rise). It should be noted here that, due to errors in the original calculation of the surface temperature, the resulting present-day ice sheet is slightly different from that presented in the supplementary information of Bentley et al. (2010). This discrepancy also has an impact on the LGM reconstructions presented in Section 5 (discussed further there), but does not affect the overall conclusion of the study.

Although the WAIS half of the domain is in good agreement, the EAIS half of the domain is not represented well. In the region of Recovery glacier, there are practically no input measurements in the BEDMAP dataset, hence, the model is not able to represent the fast flow feature which occurs in the region. The predicted ice sheet surface is approximately 1000 m too high in this region, and the morphology of the predicted ice sheet surface is very different to the measured surface (Fig. 3a and c). Le Brocq et al. (2008) inferred basal topography in this region from an analysis of ice sheet surface plan curvature. When this basal topography is incorporated into the BEDMAP dataset, the model prediction is much more successful for the EAIS, with the Recovery Glacier tributaries extending further into the inland ice sheet surface (Fig. 3e and f).

Despite the high resolution of the model domain, the flow through the Ellsworth Mountains (Minnesota Glacier) is not reproduced. As a result of this, the ice sheet surface inland of the Ellsworth Mountains is not predicted well. The ice sheet elevations are over 400 m too high, greater than the thickness difference observed in the field evidence. Nearer the grounding line (at the southern end of the range), the ice sheet elevation is predicted more reliably, where the flow regime is dominated by flow around the mountains. It should be noted, however, that there is greater drawdown from the major ice stream closest to the southern end of the Ellsworth Mountains in the model compared to the measured ice sheet surface. This is a compromise aimed at successfully reproducing other ice stream profiles across the WAIS as a whole.

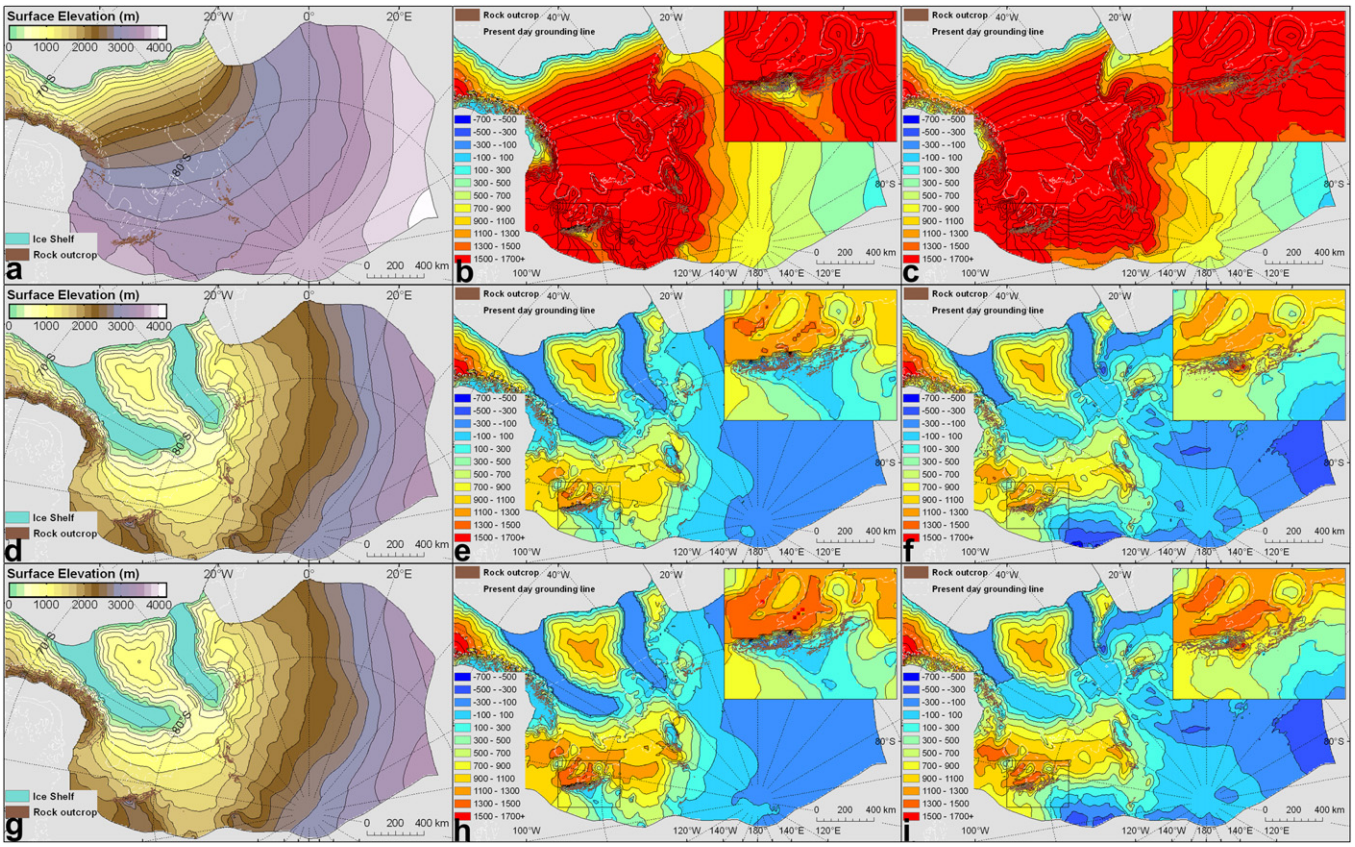

Fig. 4. LGM results; a) Experiment 1: modelled surface elevation (grounding line at shelf-break), b) Experiment 1: elevation difference with present day modelled surface, c) Experiment 1: elevation difference with present day measured surface, d) Experiment 5: modelled surface elevation, e) Experiment 5: elevation difference with present day modelled surface, f) Experiment 5: elevation difference with present day measured surface, g) Experiment 6: modelled surface elevation, h) Experiment 6: elevation difference with present day modelled surface, i) Experiment 5: elevation difference with present day measured surface.

As a result of the small differences between the measured and modelled present day ice sheet surfaces described above, comparison of LGM to present day elevation changes must be carried out in the context of both the measured and modelled present day ice sheet surfaces. To avoid any impact of model bias (impact of uncertainty in input datasets, e.g. climate or bed topography), the LGM ice sheet surface is compared with the modelled present day ice sheet surface. However, due to the small differences in the present-day modelled ice sheet surface, comparison with the measured present day ice sheet surface provides an additional check that the LGM reconstruction is also consistent with the measured present day ice elevations.

For the eustatic sea-level equivalent calculations (see Section 3.5 for calculations), the modelled present-day total ice thickness above buoyancy is used. Whilst this reduces the impact of model bias, it is important to consider its impact on the calculation compared to using the measured ice sheet surface. The modelled total ice thickness above buoyancy is the equivalent of ~0.1 m of eustatic sea-level change less than the measured total ice thickness above buoyancy.

5. LGM experiments

5.1. Experiment 1: grounding line at the shelf break

As mentioned above, there is little evidence with which to constrain the location of the grounding line at the LGM. Experiment 1 sets the grounding line at the continental shelf break. This is the maximum reasonable extent possible for the ice sheet. Previous modelling studies with a dynamic grounding line have demonstrated the relative ease with which a numerical model can predict grounded ice near or at the continental shelf break in the Weddell Sea.

The equilibrium ice sheet, resulting from the LGM climatic conditions described above and the grounding line located at the continental shelf break, is approximately 2000 m thicker than the present day ice sheet in the southern Ellsworth Mountains (Fig. 4a and b). This is thicker than that predicted by previous modelling studies (~1500 m thicker than present day), a result of the differing sliding law employed, and the equilibrium nature of the model. The eustatic sea-level equivalent of the excess ice in this modelled ice sheet is 14.1 m. The result from this model configuration suggests that either the grounding line was unlikely to be located at the continental shelf break at the LGM, or that the model applied cannot represent the ice dynamics of the sector appropriately. The main deficiency of this type of ice sheet model is the lack of a physically based representation of ice stream flow and its impact on drawing down the ice sheet surface. However, even with a more realistic ice stream model, it is hard to reconcile a 1000 km grounding line advance with only a ~480 m thickening near to the present day grounding line. The ice stream/ice plain features which would be in existence would be barely above flotation and therefore would not contribute a large amount to the eustatic sea-level equivalent. Therefore, the approach taken in the next set of experiments is to artificially lower the predicted ice sheet surface by testing different grounding line locations and comparing the resulting ice sheet surface to the field observations.

5.2. Experiments 2–9: limited expansion grounding lines

The suite of grounding lines described in Section 3.4 and Fig. 2 were implemented and the thickness difference between the LGM and present day ice sheets was examined. The following section describes the two ice sheet reconstructions which provide plausible reconstructions that fit the field evidence (Experiments 5 & 6). The grounding line locations providing the best fit are slightly less extensive compared to those presented in Bentley et al. (2010), as a result of the corrected temperature calculation. The corrected temperature calculation leads to lower surface air temperatures and, hence, a thicker ice sheet. The resulting range of eustatic sea-level equivalent values presented yield a slightly higher minimum estimate, but a similar maximum estimate, so do not change the overall conclusions of Bentley et al. (2010).

5.2.1. Experiment 5

In this experiment, the modelled LGM ice sheet is 300–500 m thicker than the modelled present day ice sheet at the southern end of the Ellsworth Mountains (Fig. 4d and e), and consistently so along the inland side of the southern Heritage Range (Fig. 4f). In the Shackleton Range, the elevation difference is slightly larger than predicted by the field evidence, approximately 100–300 m in the proximity of the mountains. The LGM elevation of the Berkner ice rise varies from 100 m thinner to 300 m thicker than present across the ice rise. The Behrendt Mountains are overridden in this experiment. The excess ice at the LGM in this experiment is equivalent to ~1.9 m of eustatic sea-level rise (compared to 1.4 m for the minimum reconstruction in Bentley et al., 2010).

There is some uncertainty over whether the large ice rise existed in the central WSE, north of Berkner ice rise, as no field data yet exist with which to test this. Without this ice rise, the eustatic sea-level equivalent for this experiment is only ~1.4 m. This is therefore the minimum estimate.

5.2.2. Experiment 6

In this experiment, the thickening at the southern end of the Ellsworth Mountains is slightly higher than Expt. 5, over 500 m thicker than both the measured and modelled present day ice sheet surface at the southern end of the Heritage Range, though in the 300–500 m range one cell width from the range itself (Fig. 4g–i). The result of this experiment indicates the maximum bound on eustatic sea-level equivalent from the model. The extent of the grounding line advance around the Shackleton Range is the same as the previous experiment. Berkner ice rise is, as in Expt. 5, between 100 m thinner and 300 m thicker across the ice rise. The increase in ice above buoyancy at the LGM in this experiment is equivalent to ~2.2 m of eustatic sea-level rise (compared to 2.0 m for the maximum reconstruction in Bentley et al., 2010).

The results from these experiments suggest that the interior ice in the WSE was up to 400 m thinner than the present day ice sheet (due to decreased snowfall). There is conflicting information available from ice core records as to the magnitude and direction of elevation change in the interior ice sheet. Analysis of air content in ice core records at the Vostok and Byrd sites suggests that the ice sheet surface was 200–300 m lower at the LGM than present (Jouzel et al., 1989; Raynaud and Whillans, 1982). However, the air content is also a function of surface atmospheric pressure, surface wind speed and the magnitude and seasonality of temperature and precipitation (Martinerie et al., 1994; Krinner et al., 2000). These other variables introduce uncertainty of the same order as the elevation changes (Krinner et al., 2000), and as they are poorly constrained cast doubt onto the inferences of elevation change from air content of ice cores. $\delta^{18}O$ records from the Byrd ice core imply that ice elevations were in fact 500–600 m higher at the LGM (Jenssen, 1983). A small thinning over a large interior area will impact on the equivalent eustatic sea-level contribution, and as there is no concrete evidence to support a thinner ice sheet, the impact of the thinner interior ice on the sea-level equivalent of the excess ice is considered further here. In their study, Denton and Hughes (2002) only considered ice elevation change below the 2000 m contour of the present day ice sheet, assuming no change above this elevation. Given the potential uncertainties associated with some elevation inferences from ice core data and since we are interested in the maximum sea-level contribution we adopt a similar approach to obtain a *maximum* estimate of 3.0 m of sea-level equivalent, assuming any modelled thinning above 2000 m elevation is ignored. Therefore, this estimate provides the maximum equivalent eustatic sea-level estimate from this study.

6. Discussion and uncertainty

A range of eustatic sea-level equivalent values has been presented here, rather than an absolute value, from a set of limited-expansion grounding line experiments. The equivalent eustatic sea-level rise due to the deglaciation of the WSE since the LGM is therefore proposed to be 1.4–3 m.

As discussed in Section 1.1, there are uncertainties attached to the approach taken in this paper, these uncertainties are considered in more detail here. The major sources of uncertainty are; a) the inadequate physics in the model, b) the location of the grounding line and c) the impact of assuming an equilibrium ice sheet. Here, we discuss each, with a specific focus on the likely impact on sea-level contribution estimates.

With respect to a), the inadequate physics in the model, the key issues are the representation of longitudinal stresses in the ice, basal sliding through sediment deformation, and a better representation of ice flow through and around mountainous areas. Most critical of these inadequacies is the representation of basal processes and the sliding relation employed in the ice flow model. A simple sliding relation, where sliding velocity is a linear function of basal shear stress (e.g. in original Glimmer model), does not reproduce the low slopes of the West Antarctic Ice Sheet. Incorporating an effective pressure term into the sliding relation improves the reproduction of the present day ice sheet presented here. However, as it is implemented here, it also indirectly introduces a water-depth related term into the sliding, and so, when the LGM grounding line is at the continental shelf break (where there are relatively shallow water depths), the model is not able to maintain extensive fast flow. It is only when the grounding line is fixed in relatively deep water that extensive fast flow is maintained. An alternative approach, with a physically based representation of basal sliding that incorporates sediment deformation and the role of subglacial water, might allow extensive fast flow to be maintained more easily in shallow water depths and may reconcile the extensive grounding line and low surface slopes required from the field evidence. Incorporating the role of subglacial water in the basal sliding relation might also help to improve the match of the modelled Berkner ice rise change to the field evidence of thickening, less meltwater provision compared to the main bulk of the ice sheet would lead to slower ice flow and cause thicker ice.

Ice flow related model inadequacies need to be addressed through the use of a higher-order, high resolution ice sheet model which incorporates a more sophisticated basal flow regime. This is a challenging task, and whilst these developments are in progress, it will be some time before they can be applied to this kind of task with confidence.

With respect to b), the modelled grounding line position in the two major troughs is only considered indicative of locations where the grounding line *might* have been. Fixing the grounding line

location as by this method is a way of forcing the model to produce low profile features in expected ice stream locations. It might be that lightly grounded ice did, in fact, exist in these troughs, but if so, these will have made a minimal contribution to sea-level change due to a low ice thickness above buoyancy. However, considering the nature of the bathymetry (Fig. 1), it makes some sense for the grounding line to be located as suggested in Fig. 4 for a period of time, as there is evidence of greater erosion (and hence grounded ice for a longer period of time) at this ice sheet extent. A snapshot from Pollard and DeConto's (2009) model at 1.094 Myr ago provides some support that this may have been a plausible grounding line.

Assumption c) relates to the fact that, in this paper, the model has been run to equilibrium (or at least a small variance around a steady state). Ice sheets take time to respond to changes in climate/sea-level forcing, so this may not be a realistic assumption. Ideally, a time-dependent 'dynamic' equilibrium would be examined, however this is not possible with the Glimmer ice sheet model due to the lack of grounding line migration and ice shelf representation.

It is important to consider the impact of this uncertainty on the potential sea-level equivalent result. A better representation of a) (in terms of an improved representation of the stress regime) and c), above, would not allow a larger ice sheet to occupy the embayment, in fact it may well lead to a reduced volume ice sheet, with lower slope profiles. Uncertainty in a) (in terms of the basal sliding representation) and b) above and could potentially lead to a small increase in ice volume, through more extensive grounded fast ice flow. However, this is likely to be ice which is close to buoyancy and, hence, would not contribute a great deal to the excess ice volume at LGM.

More investigations could in future be carried out into the extensive parameter space of this problem, i.e. grounding line location, basal sliding parameter, sensitivity to climate parameterisation. However, all the field evidence points towards minimal change in the configuration of the Weddell Sea Embayment: glacial geologic evidence of minimal thickening near the grounding lines, ice core evidence of Berkner ice rise remaining an independent ice centre and LGM flow direction indicators similar to present day. This is not consistent with an extensive, well grounded ice sheet, and requires lightly grounded fast flow features, or a less extensive grounding line. This type of ice sheet is unlikely to provide any more sea-level change equivalent than suggested here.

7. Conclusions

This paper has described, in detail, the approach taken in producing a new reconstruction of the WSE ice sheet at the LGM (proposed in Bentley et al., 2010), reconciling both ice sheet modelling results and recently derived field evidence. The field evidence suggests a thinner LGM ice sheet than had previously been considered, only ~230–480 m thicker than the present day ice sheet at the Ellsworth Mountains. The ice sheet model used here successfully reproduces the present day surface elevation of the AIS in the WSE. Allowing the grounding line to advance to the continental shelf break resulted in a ~2000 m thicker ice sheet at the LGM in the vicinity of the Ellsworth Mountains. In order to reconstruct a ~480 m thickness change in the southern Ellsworth Mountains using the numerical ice sheet model employed in this paper, the grounding line advance must be restricted in two major troughs on the continental shelf. This paper is not suggesting that this is exactly where the grounding line was located at the LGM, only that this is the grounding line required by the model to reproduce the observed LGM ice sheet configuration. The grounding line prediction is strongly a function of the nature of the numerical model applied, however, if grounded ice did exist in the two deep troughs in the Weddell Sea Embayment, it is likely to have been lightly grounded and hence not contribute a great deal to sea-level change.

The excess ice in the LGM reconstructions results in a predicted equivalent eustatic sea-level contribution of 1.4–3 m from the WSE since the LGM, lower than previous modelling based reconstructions. Despite the limitations of this approach, it is unlikely that the eustatic sea-level equivalent contribution of the deglaciation of the WSE could be any higher than 3 m. This result decreases the estimated contribution to sea-level rise, since the LGM, of this sector of the AIS, and the AIS as a whole, compared to previous modelling reconstructions. Given this low total of excess ice and the evidence for continuing deglaciation through the Holocene (Bentley et al., 2010), it follows that it is unlikely that the WSE could have contributed a large amount of sea-level rise to MWP1a. A smaller LGM ice sheet may also have implications for Antarctic mass balance calculations derived from satellite gravity data, because there will be a smaller GIA correction and hence a smaller overall ice mass loss. This latter issue requires further work to determine the magnitude of the change.

This paper has highlighted the important role of observations in constraining numerical ice sheet models, but also raised methodological issues about how this is achieved. The potential sea-level contribution was provided as a range to reflect the uncertainty and potential equifinality in the approach. Whilst we believe that this range is a realistic evaluation of the potential sea-level equivalent from the Weddell Sea, the robustness of the result could be improved through application of more advanced model physics, and more extensive bathymetric measurements.

Acknowledgments

This research was funded by NERC grant NER/G/S/2003/00020 in collaboration with NERC grant NE/EO18254/1. Thanks to Jonathan Bamber for providing the surface elevation data, Ian Joughin for providing the velocity data and two anonymous reviewers for helpful comments on the manuscript.

References

Alley, R.B., Blankenship, D.D., Bentley, C.R., Rooney, S.T., 1986. Deformation of till beneath Ice Stream B, West Antarctica. Nature 322 (6074), 57–59.

Anderson, J.B., Kurtz, D.D., Weaver, F.M., 1979. Sedimentation on the Antarctic continental slope. In: Doyle, L.J., Pilkey, O.H. (Eds.), Geology of Continental Slopes. Society of Economic Paleonlologists and Mineralogists Special Publication, vol. 27, pp. 265–283.

Anderson, J.B., Kurtz, D.D., Domack, E.W., Balshawk, M., 1980. Glacial and glacial marine sediments of the Antarctic continental shelf. Journal of Geology 88, 399–414.

Anderson, J.B., Andrews, J.T., 1999. Radiocarbon constraints on ice sheet advance and retreat in the Weddell Sea, Antarctica. Geology 27, 179–182.

Arthern, R.J., Winebrenner, D.P., Vaughan, D.G., 2006. Antarctic snow accumulation mapped using polarization of 4.3-cm wavelength microwave emission. Journal of Geophysical Research-Atmospheres 111, D06107. doi:10.1029/2004JD005667.

Bamber, J.L., Gomez-Dans, J.L., Griggs, J.A., 2009. A new 1 km digital elevation model of the Antarctic derived from combined satellite radar and laser data – Part 1: Data and methods. The Cryosphere 3, 101–111.

Bassett, S.E., Milne, G.A., Mitrovica, J.X., Clark, P.U., 2005. Ice sheet and solid earth influences on far-field sea-level histories. Science 309, 925–928.

Bassett, S.E., Milne, G.A., Bentley, M.J., Huybrechts, P., 2007. Modelling Antarctic sea-level data to explore the possibility of a dominant Antarctic contribution to meltwater pulse IA. Quaternary Science Reviews 26, 2113–2127.

Bentley, M.J., 1999. Volume of Antarctic Ice at the Last Glacial Maximum, and its impact on global sea level change. Quaternary Science Reviews 18, 1569–1595.

Bentley, M.J., Anderson, J.B., 1998. Glacial and marine geological evidence for the ice sheet configuration in the Weddell Sea Antarctic Peninsula region during the Last Glacial Maximum. Antarctic Science 10, 309–325.

Bentley, M.J., Fogwill, C.J., Kubik, P.W., Sugden, D.E., 2006. Geomorphological evidence and cosmogenic 10Be/26A1 exposure ages for the Last Glacial Maximum and deglaciation of the Antarctic Peninsula Ice Sheet. Geological Society of America Bulletin 118, 1149–1159.

Bentley, M.J., Fogwill, C.J., Le Brocq, A.M., Hubbard, A.L., Sugden, D.E., Dunai, T.J., Freeman, S., 2010. Deglacial history of the West Antarctic Ice Sheet in the Weddell Sea embayment: constraints on past ice volume change. Geology 38 (5), 411–414.

Budd, W.F., Jenssen, D., Smith, I.N., 1984. A 3-dimensional time-dependent model of the West Antarctic Ice-Sheet. Annals of Glaciology 5, 29–36.

Chen, J.L., Wilson, C.R., Tapley, B.D., Blankenship, D., Young, D., 2008. Antarctic regional ice loss rates from GRACE. Earth and Planetary Science Letters 266, 140–148.

Clark, P.U., Alley, R.B., Keigwin, L.D., Licciardi, J.M., Johnsen, S.J., Wang, H.X., 1996. Origin of the first global meltwater pulse following the last glacial maximum. Paleoceanography 11, 563–577.

Clark, P.U., Mitrovica, J.X., Milne, G.A., Tamisiea, M.E., 2002. Sea-level fingerprinting as a direct test for the source of global meltwater pulse IA. Science 295, 2438–2441.

Comiso, J.C., 2000. Variability and trends in Antarctic surface temperatures from in situ and satellite infrared measurements. Journal of Climate 13 (10), 1674–1696.

Denton, G.H., Hughes, T.J., 1981. The Last Great Ice Sheets. Wiley, New York.

Denton, G.H., Bockheim, J.G., Rutford, R.H., Andersen, B.G., 1992. Glacial history of the Ellsworth Mountains, West Antarctica. In: Webers, G.F., Craddock, C., Splettstoesser, J.F. (Eds.), Geology and Paleontology of the Ellsworth Mountains, West Antarctica. Geological Society of America, Boulder, Colorado, pp. 403–432.

Denton, G.H., Hughes, T.J., 2002. Reconstructing the Antarctic ice sheet at the Last Glacial Maximum. Quaternary Science Reviews 21, 193–202.

Elverhoi, A., 1981. Evidence for a late Wisconsin glaciation of the Weddell Sea. Nature 293, 641–642.

Fairbanks, R.G., 1989. A 17,000-year glacio-eustatic sea-level record – influence of glacial melting rates on the Younger Dryas event and deep-ocean circulation. Nature 342, 637–642.

Farrell, W.E., Clark, J.A., 1976. On postglacial sea level. Geophysical Journal of the Royal Astronomical Society 46, 647–667.

Fogwill, C.J., Bentley, M.J., Sugden, D.E., Kerr, A.R., Kubik, P.W., 2004. Cosmogenic nuclides Be-10 and Al-26 imply limited Antarctic Ice Sheet thickening and low erosion in the Shackleton Range for $>$ 1 my. Geology 32, 265–268.

Griggs, J.A., Bamber, J.L., 2009. A new 1 km digital elevation model of the Antarctic derived from combined satellite radar and laser data – Part 2: Validation and error estimates. The Cryosphere 3, 113–123.

Hanebuth, T., Stattegger, K., Grootes, P.M., 2000. Rapid flooding of the Sunda Shelf: a late-glacial sea-level record. Science 288, 1033–1035.

Hagdorn, M.K.M., 2003. Reconstruction of the Past and Forecast of the Future European and British Ice Sheets and associated sea-level change. Unpublished PhD thesis Edinburgh.

Höfle, H.-C., Buggisch, W., 1995. Glacial geology and petrography of erratics in the Shackleton Range, Antarctica. Polarforschung 63, 183–201.

Huybrechts, P., 2002. Sea-level changes at the LGM from ice-dynamic reconstructions of the Greenland and Antarctic ice sheets during the glacial cycles. Quaternary Science Reviews 21, 203–231.

Ivins, E.R., James, T.S., 2005. Antarctic glacial isostatic adjustment: a new assessment. Antarctic Science 17, 541–553.

Jenssen, D., 1983. Elevation and climatic changes from total gas content and stable isotopic measurements. In: Robin, G.d.Q. (Ed.), The Climatic Record in Polar Ice Sheets. Cambridge University Press, Cambridge, pp. 138–144.

Joughin, I., Tulaczyk, S., MacAyeal, D., Engelhardt, H., 2004. Melting and freezing beneath the Ross ice streams, Antarctica. Journal of Glaciology 50, 96–108.

Jouzel, J., Lorius, C., Petit, J.R., Genthon, C., Barkov, N.I., Kotlyakov, V.M., Petrov, V.M., 1987. Vostok Ice Core – a continuous isotope temperature record over the Last Climatic Cycle (160,000 Years). Nature 329, 403–408.

Jouzel, J., Raisbeck, G., Benoist, J.P., Yiou, F., Lorius, C., Raynaud, D., Petit, J.R., Barkov, N.I., Korotkevitch, Y.S., Kotlyakov, V.M., 1989. A comparison of deep Antarctic Ice cores and their implications for climate between 65,000 and 15,000 years ago. Quaternary Research 31, 135–150.

Krinner, G., Raynaud, D., Doutriaux, C., Dang, H., 2000. Simulations of the Last Glacial Maximum ice sheet surface climate: implications for the interpretation of ice core air content. Journal of Geophysical Research-Atmospheres 105, 2059–2070.

Lambeck, K., Nakiboglu, S.M., 1980. Seamount loading and stress in the ocean lithosphere. Journal of Geophysical Research 85, 6403–6418.

Le Brocq, A.M., Hubbard, A., Bentley, M.J., Bamber, J.L., 2008. Subglacial topography inferred from ice surface terrain analysis reveals a large un-surveyed basin below sea level in East Antarctica. Geophysical Research Letters 35, L16503. doi:10.1029/2008GL034728.

Le Meur, E., Huybrechts, P., 1996. A comparison of different ways of dealing with isostasy: examples from modelling the Antarctic ice sheet during the last glacial cycle. Annals of Glaciology 23, 309–317.

Liu, H., Jezek, K.C., Li, B., 1999. Development of an Antarctic digital elevation model by integrating cartographic and remotely sensed data: a geographic information system based approach. Journal of Geophysical Research 104, 23199–23213.

Lythe, M.B., Vaughan, D.G., the BEDMAP Consortium, 2001. BEDMAP: a new ice thickness and subglacial topographic model of Antarctica. Journal of Geophysical Research-Solid Earth 106, 11335–11351.

Martinerie, P., Lipenkov, V.Y., Raynaud, D., Chappellaz, J., Barkov, N.I., Lorius, C., 1994. Air Content Paleo Record in the Vostok Ice Core (Antarctica) – a mixed record of climatic and glaciological parameters. Journal of Geophysical Research-Atmospheres 99, 10565–10576.

Maule, C.F., Purucker, M.E., Olsen, N., Mosegaard, K., 2005. Heat flux anomalies in Antarctica revealed by satellite magnetic data. Science 309, 464–467.

Mulvaney, R., Arrowsmith, C., Barnola, J.M., McCormack, T., Loulergue, L., Raynaud, D., Lipenkov, V.Y., Hindmarsh, R.C.A., 2007. A deglaciation climate and ice sheet history of the Weddell Sea region from the Berkner Island ice core. Quaternary International 167–168 (Supplement 1), 294–295.

Parrenin, F., Dreyfus, G., Durand, G., Fujita, S., Gagliardini, O., Gillet, F., Jouzel, J., Kawamura, K., Lhomme, N., Masson-Delmotte, V., Ritz, C., Schwander, J., Shoji, H., Uemura, R., Watanabe, O., Yoshida, N., 2007. 1-D-ice flow modelling at EPICA Dome C and Dome Fuji, East Antarctica. Climate of the Past 3, 243–259.

Payne, A., Sugden, D., 1990. Topography and ice-sheet growth. Earth Surface Processes and Landforms 15, 625–639.

Payne, A.J., 1999. A thermomechanical model of ice flow in West Antarctica. Climate Dynamics 15, 115–125.

Philippon, G., Ramstein, G., Charbit, S., Kageyama, M., Ritz, C., Dumas, C., 2006. Evolution of the Antarctic ice sheet throughout the last deglaciation: a study with a new coupled climate – north and south hemisphere ice sheet model. Earth and Planetary Science Letters 248, 750–758.

Pollard, D., DeConto, R.M., 2009. Modelling West Antarctic ice sheet growth and collapse through the past five million years. Nature 458 (7236), 329–333.

Ramilllien, G., Lombard, A., Cazenave, A., Ivins, E.R., Llubes, M., Remy, F., Biancale, R., 2006. Interannual variations of the mass balance of the Antarctica and Greenland ice sheets from GRACE. Global and Planetary Change 53, 198–208.

Raynaud, D., Whillans, I.M., 1982. Air content of the Byrd core and past changes in the West Antarctic Ice Sheet. Annals of Glaciology 3, 269–273.

Rippin, D.M., Siegert, M.J., Bamber, J.L., Vaughan, D.G., Corr, H.F.J., 2006. Switch-off of a major enhanced ice flow unit in East Antarctica. Geophysical Research Letters 33, L15501. doi:10.1029/2006GL026648.

Ritz, C., Rommelaere, V., Dumas, C., 2001. Modeling the evolution of Antarctic ice sheet over the last 420,000 years: implications for altitude changes in the Vostok region. Journal of Geophysical Research-Atmospheres 106, 31943–31964.

Ruth, U., Barnola, J.M., Beer, J., Bigler, M., Blunier, T., Castellano, E., Fischer, H., Fundel, F., Huybrechts, P., Kaufmann, P., Kipfstuhl, S., Lambrecht, A., Morganti, A., Oerter, H., Parrenin, F., Rybak, O., Severi, M., Udisti, R., Wilhelms, F., Wolff, E., 2007. "EDML1": a chronology for the EPICA deep ice core from Dronning Maud Land, Antarctica, over the last 150 000 years. Climate of the Past 3, 475–484.

Rutt, I.C., Hagdorn, M., Hulton, N.R.J., Payne, A., 2009. The 'Glimmer' community ice sheet model. Journal of Geophysical Research-Earth Surface 114, F02004. doi:10.1029/2008JF001015.

Sasgen, I., Martinec, Z., Fleming, K., 2007. Regional ice-mass changes and glacial-isostatic adjustment in Antarctica from GRACE. Earth and Planetary Science Letters 264, 391–401.

Schoof, C., 2007. Ice sheet grounding line dynamics: Steady states, stability, and hysteresis. Journal of Geophysical Research 112 (F3), F03S28. doi:10.1029/2006JF000664.

Steig, E.J., Morse, D.L., Waddington, E.D., Stuiver, M., Grootes, P.M., Mayewski, P.A., Twickler, M.S., Whitlow, S.I., 2000. Wisconsinan and Holocene climate history from an ice core at Taylor Dome, western Ross Embayment, Antarctica. Geografiska Annaler Series a-Physical Geography 82A, 213–235.

Stenni, B., Masson-Delmotte, V., Johnsen, S., Jouzel, J., Longinelli, A., Monnin, E., Rothlisberger, R., Selmo, E., 2001. An oceanic cold reversal during the last deglaciation. Science 293, 2074–2077.

Taylor, K.C., White, J.W.C., Severinghaus, J.P., Brook, E.J., Mayewski, P.A., Alley, R.B., Steig, E.J., Spencer, M.K., Meyerson, E., Meese, D.A., Lamorey, G.W., Grachev, A., Gow, A.J., Barnett, B.A., 2004. Abrupt climate change around 22 ka on the Siple Coast of Antarctica. Quaternary Science Reviews 23, 7–15.

Tulaczyk, S., Kamb, W.B., Engelhardt, H.F., 2000. Basal mechanics of Ice Stream B, West Antarctica 1. Till mechanics. Journal of Geophysical Research-Solid Earth 105 (B1), 463–481.

Velicogna, I., 2009. Increasing rates of ice mass loss from the Greenland and Antarctic ice sheets revealed by GRACE. Geophysical Research Letters 36, L19503. doi:10.1029/2009GL040222.

Velicogna, I., Wahr, J., 2006. Measurements of time-variable gravity show mass loss in Antarctica. Science 311, 1754–1756.

Vialov, S.S., 1958. Regularities of glacial shields movement and the theory of plastic viscous flow. IAHS Publications 47, 266–275.

Weertman, J., 1964. The theory of glacier sliding. Journal of Glaciology 5, 287–303.